# Causes of Degradation Identified by the Extended Thermal Cycling Test on Commercially Available Crystalline Silicon Photovoltaic Modules

Shinji Kawai [ID], Tadanori Tanahashi [ID], Yutaka Fukumoto [ID], Fujio Tamai [ID], Atsushi Masuda, and Michio Kondo

*Abstract*—To assess the contribution of the thermomechanical stress on the long-term reliability of photovoltaic (PV) modules, we applied extended thermal cycling tests up to 600 cycles to 13 models of commercially available PV modules. The extensive testing, using 5–10 PV modules for each model, revealed that the levels of power loss, induced by thermal fatigue during this extended testing, differed in each model of the PV module. Degradations by solder bond failure and bypass diode failure, which were observed in a few models of PV modules, were most likely to result from incorrect soldering that may be completely avoidable through appropriate implementation of a quality management system. Therefore, we suggest that, in most of the latest PV modules, their durability to thermal fatigue was established, as evidenced by the extended thermal cycling test with 600 cycles. However, solder bond failure due to inappropriate manufacturing process quality, which is not identifiable by the conventional thermal cycling test (200 cycles), would be detected by this extended test in a few models. Based on these suggestions, we discuss the evaluation procedures of these failures caused by the quality-control and design issues of PV modules.

*Index Terms*—Photovoltaic (PV) module reliability, quality management, solder bond failure, thermal cycling test.

## I. INTRODUCTION

THE contribution of photovoltaic (PV) solar energy to the entire electricity demand of the world has surpassed 1.2%, as reported in the recent IEA report [1]. Current trends of PV penetration will be aided by the comprehensive policy for global warming countermeasure, in accordance with the "Paris Agreement" in COP21. In order to accelerate PV deployment, the long-term reliability of PV modules is a crucial factor to reduce the life-cycle costs of PV electricity [2], [3]. We have conducted extensive testing on the durability of commercially available PV modules that were designed and manufactured in the early

2010s, in order to enhance our understanding of the current status of the long-term reliability of these PV modules. In this paper, the actual degradation profiles of 13 types of modules were investigated by exposing them to extended thermal cycling tests. The causes of degradation identified by this testing are discussed.

For crystalline silicon (c-Si) PV modules exposed outdoor over 20 years, solder damage between interconnecting ribbons and busbars on the PV cells was reported earlier [4]–[12], which was detected by an increase in the series resistance ($R_s$) in PV module circuit, infrared (IR) imaging, and/or electroluminescence (EL) imaging. Although the quality improvement of c-Si PV modules produced after 2000 was confirmed by a reduced variation of reported degradation rates [13], it was also reported that such degradation induced by solder bond failure was still observed in the c-Si PV modules that were manufactured after 2000 and were exposed for 5–10 years, even in the temperate climate of Japan [8], [10].

To evaluate the durability/reliability of c-Si PV modules with regards to this failure mode, several modifications of the acceleration test were proposed aimed at generating the thermal fatigue as a major cause of solder bond failure [14]–[23]. All of the published modifications involve an extended thermal cycling test as the extension of the cycling numbers defined in the IEC standards (IEC 61215) [24]. However, the relationship of increasing cycle numbers with the lifetime of PV modules was not experimentally established at all although it was reported that the application of 500 cycles in the thermal cycling test corresponds to 20 years of exposure of the c-Si PV modules, according to a manufacturer's experience [15]. In nearly all previous reports, it was difficult to obtain statistically supported characteristics of reliability for each model tested because the degradation effects caused by these extended thermal cycling tests were not indicated with the variance of generated electrical power for each type of model. Therefore, we have examined the extended thermal cycling test for multiple modules for each model, in order to elucidate the impact of larger sample sizes

## II. EXPERIMENTAL DETAILS

### A. PV Modules

A total of 13 models (5 or 10 PV modules for each model) of commercially available c-Si PV modules (180–235 Wp) were purchased from PV manufacturers in Japan, China,

TABLE I
EVOLUTION OF PV PARAMETERS* DURING THERMAL CYCLING TEST

| # | Model ID | c-Si | Size** | TC*** | $P_{\max}$ (W) | $I_{sc}$ (A) | $V_{oc}$ (V) | FF (%) |
|---|----------|------|--------|-------|----------------|--------------|--------------|--------|
| 1 | A | Multi | 5 | 0 | 186.97 ± 0.74 | 8.45 ± 0.02 | 29.58 ± 0.05 | 74.9 ± 0.3 |
|   |   |       | 5 | 200 | 186.28 ± 0.38 | 8.45 ± 0.03 | 29.52 ± 0.03 | 74.9 ± 0.3 |
|   |   |       | 5 | 400 | 185.18 ± 0.41 | 8.44 ± 0.03 | 29.43 ± 0.03 | 74.7 ± 0.3 |
|   |   |       | 5 | 600 | 184.61 ± 0.41 | 8.44 ± 0.03 | 29.40 ± 0.02 | 74.5 ± 0.3 |
| 2 | B | Multi | 10 | 0 | 229.61 ± 0.93 | 8.32 ± 0.02 | 36.97 ± 0.07 | 74.6 ± 0.3 |
|   |   |       | 10 | 200 | 222.25 ± 0.87 | 8.16 ± 0.02 | 36.65 ± 0.07 | 74.3 ± 0.2 |
|   |   |       | 10 | 400 | 222.30 ± 0.86 | 8.17 ± 0.02 | 36.67 ± 0.07 | 74.2 ± 0.3 |
|   |   |       | 10 | 600 | 223.68 ± 0.81 | 8.21 ± 0.02 | 36.84 ± 0.06 | 74.0 ± 0.3 |
| 3 | C | Multi | 10 | 0 | 230.90 ± 1.14 | 8.30 ± 0.02 | 36.80 ± 0.14 | 75.6 ± 0.3 |
|   |   |       | 10 | 200 | 225.62 ± 1.24 | 8.23 ± 0.03 | 36.54 ± 0.13 | 75.1 ± 0.4 |
|   |   |       | 10 | 400 | 224.39 ± 1.27 | 8.20 ± 0.03 | 36.53 ± 0.14 | 74.9 ± 0.4 |
|   |   |       | 10 | 600 | 224.13 ± 1.21 | 8.18 ± 0.03 | 36.64 ± 0.14 | 74.7 ± 0.5 |
| 4 | E | Multi | 5 | 0 | 186.83 ± 2.26 | 8.48 ± 0.06 | 29.76 ± 0.10 | 74.0 ± 0.3 |
|   |   |       | 5 | 200 | 183.40 ± 2.89 | 8.42 ± 0.07 | 29.65 ± 0.13 | 73.4 ± 0.4 |
|   |   |       | 5 | 400 | 157.70 ± 32.71 | 8.40 ± 0.06 | 26.38 ± 4.49 | 70.8 ± 4.4 |
|   |   |       | 3 | 600 | 160.90 ± 36.34 | 8.36 ± 0.04 | 26.42 ± 5.47 | 72.6 ± 1.5 |
| 5 | F | Mono | 5 | 0 | 208.88 ± 0.36 | 8.29 ± 0.02 | 33.59 ± 0.02 | 75.0 ± 0.3 |
|   |   |       | 5 | 200 | 207.01 ± 1.11 | 8.32 ± 0.03 | 33.61 ± 0.03 | 74.0 ± 0.6 |
|   |   |       | 5 | 400 | 206.24 ± 1.00 | 8.29 ± 0.03 | 33.57 ± 0.04 | 74.2 ± 0.5 |
|   |   |       | 5 | 600 | 206.67 ± 1.30 | 8.28 ± 0.02 | 33.67 ± 0.06 | 74.1 ± 0.4 |
| 6 | G | Multi | 5 | 0 | 234.12 ± 0.94 | 8.30 ± 0.04 | 37.03 ± 0.09 | 76.2 ± 0.4 |
|   |   |       | 5 | 200 | 228.83 ± 1.20 | 8.24 ± 0.05 | 36.79 ± 0.10 | 75.5 ± 0.4 |
|   |   |       | 5 | 400 | 228.06 ± 1.47 | 8.19 ± 0.04 | 36.84 ± 0.10 | 75.6 ± 0.5 |
|   |   |       | 5 | 600 | 227.56 ± 1.59 | 8.22 ± 0.04 | 36.86 ± 0.11 | 75.1 ± 0.6 |
| 7 | H | Mono | 5 | 0 | 221.51 ± 0.23 | 5.62 ± 0.01 | 51.67 ± 0.03 | 76.3 ± 0.2 |
|   |   |       | 5 | 200 | 226.79 ± 0.32 | 5.61 ± 0.01 | 52.57 ± 0.03 | 77.0 ± 0.2 |
|   |   |       | 5 | 400 | 225.62 ± 0.39 | 5.61 ± 0.01 | 52.50 ± 0.05 | 76.6 ± 0.1 |
| 8 | I | Multi | 5 | 0 | 235.58 ± 0.27 | 8.50 ± 0.02 | 37.26 ± 0.06 | 74.4 ± 0.1 |
|   |   |       | 5 | 200 | 226.82 ± 1.68 | 8.36 ± 0.02 | 36.94 ± 0.14 | 73.4 ± 0.3 |
|   |   |       | 5 | 400 | 221.46 ± 3.57 | 8.35 ± 0.02 | 36.97 ± 0.10 | 71.7 ± 1.1 |
|   |   |       | 5 | 600 | 201.44 ± 11.50 | 8.34 ± 0.03 | 36.95 ± 0.06 | 65.4 ± 4.1 |
| 9 | J | Multi | 5 | 0 | 227.99 ± 1.18 | 8.35 ± 0.04 | 36.97 ± 0.16 | 73.9 ± 0.3 |
|   |   |       | 5 | 200 | 221.01 ± 2.12 | 8.24 ± 0.06 | 36.72 ± 0.19 | 73.0 ± 0.4 |
|   |   |       | 5 | 400 | 221.96 ± 1.66 | 8.26 ± 0.06 | 36.86 ± 0.19 | 72.9 ± 0.4 |
| 10 | K | Multi | 5 | 0 | 238.77 ± 0.71 | 8.69 ± 0.02 | 37.09 ± 0.04 | 74.1 ± 0.2 |
|   |   |       | 5 | 200 | 230.98 ± 0.56 | 8.57 ± 0.04 | 36.79 ± 0.05 | 73.3 ± 0.5 |
|   |   |       | 5 | 400 | 229.04 ± 2.01 | 8.59 ± 0.04 | 36.92 ± 0.03 | 72.3 ± 0.8 |
|   |   |       | 5 | 600 | 223.37 ± 6.71 | 8.59 ± 0.05 | 36.90 ± 0.08 | 70.5 ± 1.9 |
| 11 | M | Multi | 5 | 0 | 180.91 ± 0.66 | 8.35 ± 0.05 | 29.49 ± 0.11 | 73.5 ± 0.9 |
|   |   |       | 5 | 200 | 177.78 ± 0.79 | 8.25 ± 0.05 | 29.38 ± 0.11 | 73.3 ± 0.7 |
|   |   |       | 5 | 400 | 176.60 ± 0.57 | 8.36 ± 0.04 | 29.48 ± 0.13 | 71.7 ± 0.7 |
|   |   |       | 5 | 600 | 176.73 ± 0.61 | 8.27 ± 0.03 | 29.52 ± 0.13 | 72.4 ± 0.6 |
| 12 | N | Multi | 5 | 0 | 194.85 ± 0.71 | 8.41 ± 0.03 | 30.76 ± 0.07 | 75.3 ± 0.2 |
|   |   |       | 5 | 200 | 193.88 ± 1.20 | 8.33 ± 0.03 | 30.70 ± 0.08 | 75.8 ± 0.3 |
|   |   |       | 5 | 400 | 193.32 ± 0.98 | 8.35 ± 0.05 | 30.65 ± 0.07 | 75.5 ± 0.4 |
|   |   |       | 5 | 600 | 193.29 ± 1.09 | 8.36 ± 0.06 | 30.68 ± 0.07 | 75.4 ± 0.5 |
| 13 | O | Multi | 5 | 0 | 205.53 ± 0.48 | 8.27 ± 0.01 | 33.37 ± 0.03 | 74.4 ± 0.1 |
|   |   |       | 5 | 200 | 202.75 ± 0.45 | 8.22 ± 0.02 | 33.32 ± 0.03 | 74.0 ± 0.1 |
|   |   |       | 5 | 400 | 201.67 ± 0.86 | 8.21 ± 0.01 | 33.25 ± 0.05 | 73.9 ± 0.2 |
|   |   |       | 5 | 600 | 199.76 ± 0.80 | 8.19 ± 0.01 | 33.25 ± 0.04 | 73.4 ± 0.2 |

*These parameters were determined using a solar simulator under the standard test condition (25 °C, 1000 W/m$^2$, air mass = 1.5), and these were expressed as mean value ± standard deviation.
**Size indicates the sample size in each model.
***TC denotes the cycle number of thermal cycling test.

Taiwan, South Korea, and Germany. These PV modules were manufactured in 2011 or 2012 (according to their attached nameplate), and as such they reflect recent design and manufacturing processes, i.e., we tested the "latest models of PV modules." Hereafter, the models are referred to as "model A" to "model O" for convenience in recognition (see Table I). Within these models, "model F" and "model H" incorporated mono-c-Si PV cells while the other models consisted of multi-c-Si PV cells (156 × 156 mm). All the models were constructed using the conventional architecture (front glass—encapsulant—PV cell—encapsulant—backsheet structure); the PV modules with double glass configurations were not included in these models.

## B. Extended Thermal Cycling Test

The PV modules described above were exposed to the conventional thermal cycling test conditions, in full accordance with the international standards (IEC 61215: 2005, Clause 10.11) [24]. The cumulative cycling number of this thermal cycling test was 600 cycles; however, the PV modules were taken out from the environmental test chambers (ESPEC MS-4050) every 200 cycles to assess their performance and appearance.

## C. Characterization of PV Modules

The electrical parameters ($P_{max}$: maximum generated electric power, $V_{oc}$: voltage under the open circuit condition, $I_{sc}$: current under the short circuit condition, and FF: fill factor) of these PV modules under standard test conditions, as defined in IEC TS 61816: 2016 (25 °C, 1000 W/m$^2$, air mass = 1.5 [25]), were evaluated from the current–voltage (*I–V*) curves under irradiation from a pulsed solar simulator (class AAA). Additional parameters (*n*: diode factor, $R_s$, and $R_{sh}$: shunt resistance) were extracted using Zhang's procedure modified by Suzuki *et al.* based on these *I–V* data [26], [27]. The power loss caused by the evolution of the respective electrical parameters ($I_{sc}$, $V_{oc}$, *n*, $R_s$, or $R_{sh}$) was evaluated using the method described in our previous paper [27]. IR and EL imaging were carried out using a thermo-viewer (NEC Avio H2630) and an EL imaging system (Nikon D7000 with power supplier), respectively. The obtained EL images were processed using ImageJ software (National Institute of Health, USA) to clear up the bright and dark areas observed in the EL images, by pseudo-color mapping [28].

## III. RESULTS

## A. Degradation of Commercially Available PV Modules During the Extended Thermal Cycling Test

We conducted the extended thermal cycling test on 13 models of recently designed and manufactured PV modules, in order to measure the degradation induced by the accumulation of thermal fatigue. As summarized in Table I and Fig. 1, the power loss of 10 out of the 13 models was less than 5%, even after the application of 600 cycles. Additionally, we confirmed that the variation in power loss was relatively small within these models. However, an obvious degradation greater than 5% of $P_{max}$ was observed in three models (models E, I, and K). These degradations were evident after 400 or 600 cycles with a large variance in power loss. Although the yellowing in the backsheet was observed in two models (models A and C) with an increasing cycling number, these discolorations did not cause any power loss. Slight cracks of the backsheet around the junction box were detected in four modules (within the ten modules tested) of model B at 600 cycles. Although this failure may raise a crucial safety issue, it did not cause any appreciable power loss. The results obtained for the intravariance in performance (including a safety issue) of each PV model, which were observed during the extended thermal cycling test, show that several samples in each PV model are required to reach a judgment of the assurance of PV module reliability, and that testing a single or a couple of modules is not sufficient.
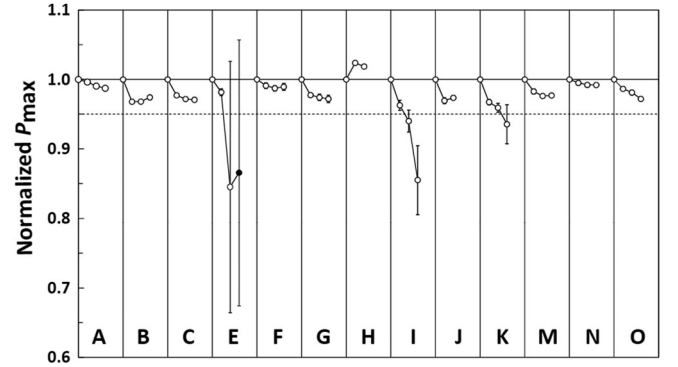


Fig. 1. Degradation profiles of commercially available PV modules during the extended thermal cycling test. The letters (A to O) indicate the model ID of the tested PV modules. The circles designate the levels (mean ± standard deviation) of $P_{max}$ normalized by the initial $P_{max}$ of each model, and corresponding to 0, 200, 400, and 600 cycles in an order from the left of each column. As the level of $P_{max}$ at 600 cycles in model E was determined by values obtained from three modules (see Fig. 2), this symbol is closed, in order to be distinguished from others. The dashed horizontal line denotes the pass/fail criteria (0.95) defined in IEC 61215.
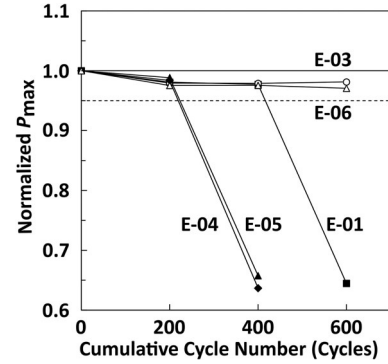


Fig. 2. Degradation profile of tested PV modules corresponding to model E during the extended thermal cycling test. Vertical axis indicates $P_{max}$ normalized by the initial $P_{max}$ of each module, and the dashed horizontal line denotes the pass/fail criteria (0.95) defined in IEC 61215.

## B. Bypass Diode Failure Observed During the Extended Thermal Cycling Test

In the most degraded PV model (model E), even though the value of $P_{max}$ was retained up to 200 cycles, as shown in Fig. 1, significant degradation was exhibited and the variance of power loss was increased at 400 and 600 cycles. The individual power loss profiles of the five tested modules of model E are shown in Fig. 2. Although the power of two modules (modules E-03 and E-06) retained over 95% even at 400 and 600 cycles, one-third of $P_{max}$ was lost in the other three modules. The typical *I–V* curves that were measured in the initial state and after 600 cycle tests for module E-01 are shown in Fig. 3. These curves obviously indicate a remarkable reduction of $V_{oc}$, but not $I_{sc}$ and FF. Module E consists of 60 cells divided into three pairs of cell-strings with bypass diodes. In three damaged PV modules (E-01, −04, and −05), the completely dark area corresponding to one pair of the PV cell-strings was confirmed using the EL image (see Figs. 4 and 5). These observations indicate the power loss caused by the shunted bypass diode or by the complete breakdown in current flow within these
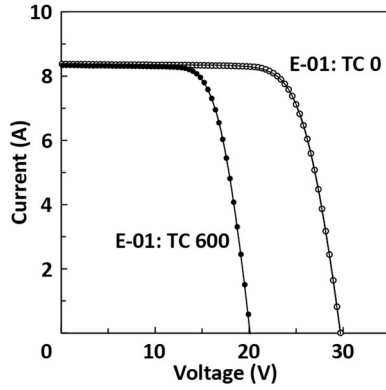
Fig. 3. *I–V* curves of module E-01 at 0 and 600 cycles under the thermal cycling test conditions. The lines in this figure indicate the fitted curves that are determined by *I--V* parameters extracted from their *I--V* data.
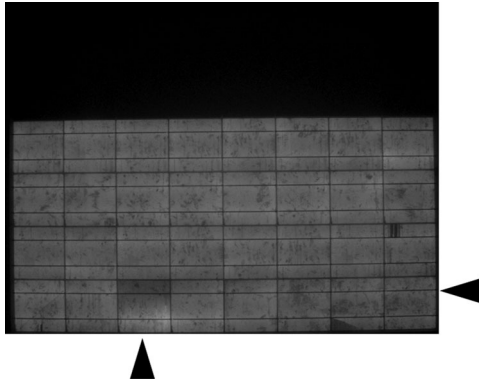


Fig. 4. EL image of module E-04 (at 400 cycles). In a PV cell located at the cross-points of the arrowheads, nonuniform distribution of the dark EL area within the PV cell is confirmed. In addition, no EL brightness is observed in the top two cell-strings of this PV module.
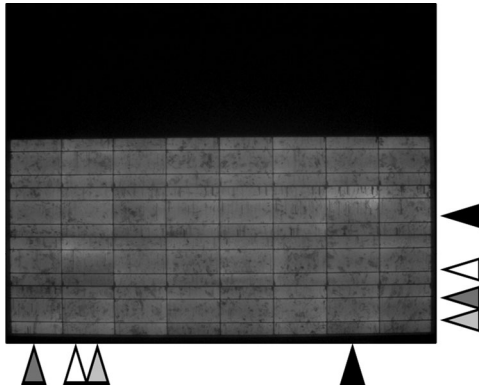


Fig. 5. EL image of module E-05 (at 400 cycles). In each PV cell located at the cross-points of the paired arrowheads with the same shaded-level, nonuniform distribution of dark EL areas within the PV cell is confirmed. In addition, no EL brightness is observed in the top two cell-strings of this PV module.

cell-strings. Indeed, when we checked the bypass diodes in these modules, using a digital multimeter after each junction box was opened, both bypass diodes, within the combination using two diodes for each PV cell-string, were shunted. In addition, the brightness of EL has diminished in half the area of several PV cells in the two damaged PV modules (E-04 and E-05), even within the brightness-retaining cell-strings of these
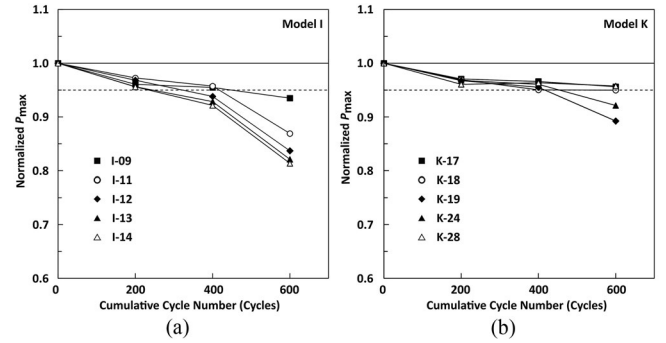


Fig. 6. Degradation profiles of tested PV modules belonging to models I and K during the extended thermal cycling test. Vertical axis indicates $P_{\max}$ normalized by the initial $P_{\max}$ of each module, and the dashed horizontal line denotes the pass/fail criteria (0.95) defined in IEC 61215.

PV modules (see Figs. 4 and 5). This observation suggests that solder bond failure occurred in these PV cells, prior to (or in parallel to) the failure of the bypass diode. On the other hand, the same model of junction box, with identical bypass diodes, was utilized in another tested model (model C), and very little power loss in all ten PV modules of model C was detected after extended thermal cycling test (600 cycles), as shown in Fig. 1. Therefore, this bypass diode failure could be ascribed to a precedent solder-bond failure since the bypass diodes used in models C and E have comparable durability to both thermal fatigue and/or high temperatures. We speculate that the value of $R_s$ increased by the solder-bond failure in a cell-string, leading to the unintentional damage of the bypass diode by the excess reverse voltage across it because the $I_{\rm sc}$ current to the PV module was constantly applied when the module temperature was higher than 25 °C during the thermal cycling test.

### C. Solder Bond Failure Observed During the Extended Thermal Cycling Test

Moderate power loss during the extended thermal cycling test was also observed in 2 models (models I and K), as shown in Fig. 1. In these models, the levels of power loss after 600 cycles were $-14.5 \pm 4.9\%$ and $-6.5 \pm 2.8\%$ for models I and K, respectively, which were lower than that caused by the bypass diode failure (model E), and their standard deviations are relatively small. The degradation profiles of models I and K (five modules each), during the extended thermal cycling test, are indicated in Fig. 6. Although each of the five modules was linearly degraded up to 400 cycles, the degradation of four and two modules was accelerated beyond that, in models I and K, respectively. The extent of power loss at 600 cycles varied in a range of $-6.5\%$ to $-18.6\%$ and $-4.2\%$ to $-10.8\%$ within each of the five modules of models I and K, respectively. These results indicate that the degradation by thermal fatigue was extensively enhanced after 400 cycles of the thermal cycling test. Furthermore, because the degradation level of each module significantly diverged, even in the same model after 600 cycles, there is a risk that testing only one or two module(s) cannot provide confidence in the degradation behavior of the PV model.
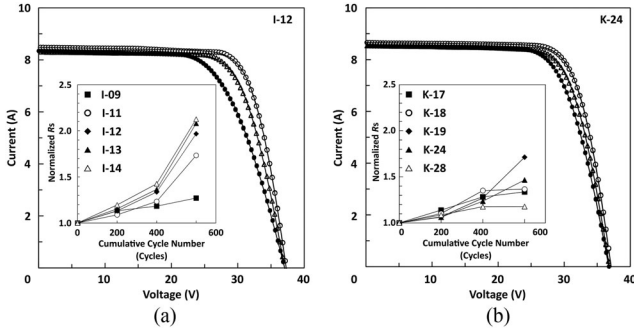
(a)             (b)

Fig. 7. *I–V* curves of module I-12 and module K-24 at 0 (open circle), 400 (open triangle), and 600 (closed circle) cycles under the thermal cycling test conditions. The lines in these figures indicate the fitted curves that are determined by *I–V* parameters extracted from their *I–V* data. Trends on the estimated $R_s$ of each PV module during this thermal cycling are drawn in the insets of these figures, in which the vertical axis denoted $R_s$ normalized by the initial $R_s$ value of each PV module.
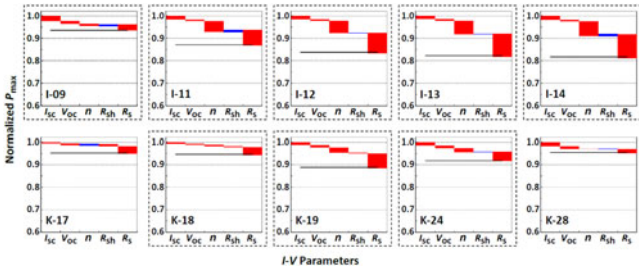


Fig. 8. Contributions of each *I–V* parameter to the power loss after 600 cycles of thermal cycling test. The name of each module name consists of the model ID and module ID and is denoted in lower left in each panel. In each panel, the amount of downward contribution of the *I–V* parameter to the electric power generation is indicated by the red band, and that of the upward contribution is shown by the blue band. These contributions are accumulated and demonstrated as a breakdown chart in each panel. Normalized $P_{\max}$ assessed by using a solar simulator is displayed as a horizontal line in each panel. PV modules with more than 5% power loss are enclosed in box with dashed line.

As shown in Fig. 7, the values of $I_{\rm sc}$ and $V_{\rm oc}$ did not significantly change with an increasing number of cycles although FF noticeably decreased and $R_s$ increased. However, $R_{\rm sh}$ normalized to an initial value was estimated to be in the range of 0.5–2.8 after 600 cycles in all modules of model I and model K. The contribution of the varied $R_{\rm sh}$ to the power loss is not crucial against those of $R_s$ and *n* (see Fig. 8), especially in the PV modules with more than 5% power loss. As discussed in previous reports [27], [29], the increase in *n* is an apparent effect caused by the nonuniform distribution of $R_s$ within PV cells in each module.

This nonuniform distribution of $R_s$ was confirmed by EL and IR images, as demonstrated in Fig. 9. In the EL images of model I, evidently darker regions were observed over one-half of the cell area in several cells after 400 cycles; the number of affected cells increased after 600 cycles. For model K, those PV cells with a darker EL region were not evident after 400 cycles but were significantly appreciable after 600 cycles. It is assumed that this increasing number of PV cells with dark EL regions may be the cause of the accelerated power loss and the increased $R_s$, indicated in Figs. 6 and 7, respectively. In the IR images shown in Fig. 9, it was found that the low-temperature areas correspond
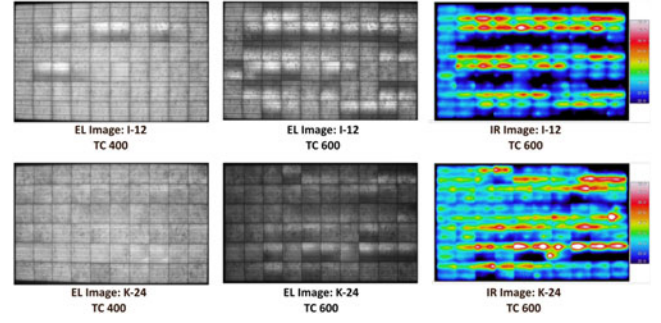


Fig. 9. EL and IR images of model I (module I-12) and model K (module K-24) at 400 and 600 cycles under the extended thermal cycling test. The colored bars in the right side of the IR images indicate the temperature range (22–30 °C).
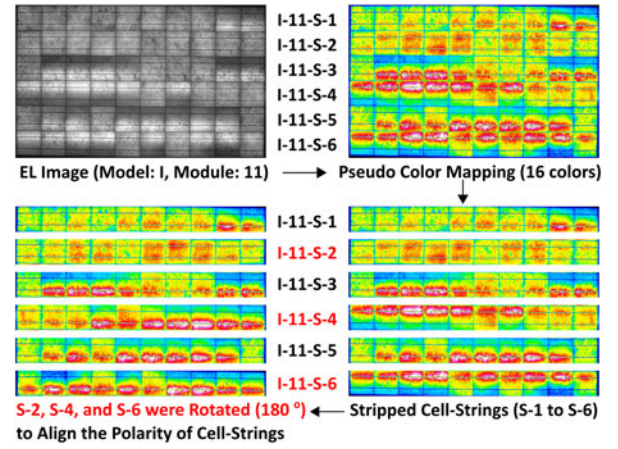


Fig. 10. EL image processing: pseudo-color mapping and polarity alignment of cell-strings. The caption for each cell-string shows the details of the cell-string in the following order: model ID (I), module ID (11), and string ID (S-1 to S-6). Red letters in these captions indicate the rotated cell-strings to align the electric polarity. For more detail, see Section III-D.

to the dark EL regions, and that the higher temperature areas were distributed across the other half of dark EL region within the affected PV cells. These results indicate that the solder bond failure on the busbar of the PV cell causes depletion of current without Joule heating and current crowding in the counterpart because other defects, such as cell cracks, break of finger grid, and interconnector breakdown, were seldom detected.

## D. Identification of Primary Cause of Degradation Observed in the Extended Thermal Cycling Test

To investigate the cause of the solder bond failure observed in the extended thermal cycling test, we studied the pattern of EL dark areas in each PV cell-string of model I because a typical solder bond failure occurred in almost all of the modules of model I as shown in Fig. 10. Prior to the pattern classification, EL images of four modules in model I (module I-09 was excluded because the clear dark EL areas were not apparent) were modified by the pseudo-color mapping. Clear color images, depending on the brightness of the EL image, were obtained as shown in the upper part of Fig. 10. The string number (S-1 to S-6) was allocated in each cell-string from the upper side of the module that was placed with the junction box positioned at the
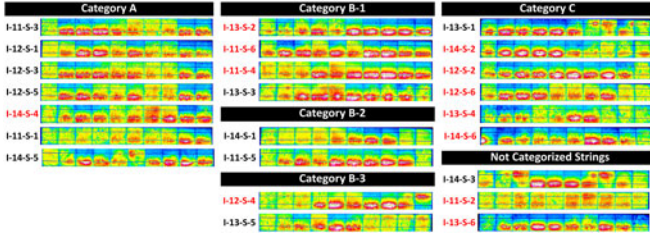
Fig. 11.   Cell-strings categorized by EL brightness. The caption for each cell-string shows the details of the cell-string in the following order: model ID (I), module ID (11, 12, 13, or 14), and string ID (S-1 to S-6). Cell-string with distinctive characteristics of each category is deployed more upper portion within each category.

left side as viewed from the front of module (upper right panel of Fig. 10). These cell-strings were then "cut" into strips as picture images (lower right panel of Fig. 10). Subsequently, to align the polarity of these cell-strings, the even-numbered cell-strings (S-2, S-4, and S-6) were rotated 180° (as indicated in the lower left panel of Fig. 10). The pictures of the aligned cell-strings with the name consisting of model ID (I), module ID (11, 12, 13, and 14), and string ID (S-1 to S-6) were put together, and were categorized by the similarity of picture pattern originating from the EL brightness in order to confirm the cause of solder bond failure. If a similar pattern was often observed in some modules within one PV model, the existence of a common failure-cause in the soldering process of this model would be suggested.

Every cell-string of four modules in model I is shown in Fig. 11. It is evident that the mostly blue/green areas (equivalent to the dark area in the EL image) were positioned in the upper portion of each cell-string. In addition, by the difference in the intrastring distribution of the remaining intact-area (observed as yellow/red area) in the upper portion of each cell, these cell-strings were divided into four categories (Category A: the intact area was distributed around the left and central cells within these cell-strings, category B: the intact area was unevenly distributed in the left half of the cell-strings, and category C: the intact area was mainly distributed in the right half of cell-strings, and not categorized strings). For category B, the three subcategories were featured because some cell-strings may be located in the intercategory position. Of note is the fact that all categories consisted of cell-strings originating from two or three modules; however, these failures would be derived from multiple string-machines with poor adjustment since the unidirectional evolution of the EL images through these categories was not identified. Therefore, it is indicated that this failure was most probably due to a common root cause, i.e., the poor adjustment of the soldering machines used in the cell-stringing process.

## IV. Discussion

We demonstrated in this study, even in recently designed and manufactured PV modules that were purchased from the market, some solder bond failure between the busbar and interconnecting ribbon on PV cells were detected only by an extended thermal cycling test. However, this failure was quite probably a quality issue caused by poor manufacturing process controls.

As summarized in Section I, the extension of the number of cycles in the thermal cycling test was proposed based on the analysis of a few commercially available PV modules. Although this approach seems to be useful for the establishment of an appropriate module design and soldering process, it is not sufficient to establish the confident rating-protocols for quality assurances accepted by all stakeholders (PV cell/module manufacturers, PV system engineers, PV plant/residential-use owners, investors, and others). This is because the approach does not consider the durability-variance within the model of PV modules. However, in our tests that use 5–10 PV modules for each model, it became evident that a large variance of susceptibility to thermal fatigue is observed within a single model, as described in Section III-A. Therefore, multiple test-samples (more than five modules) are required in the precise quality-evaluation for models of PV modules for practical purposes, as proposed by the International PV Quality Assurance Task Force [30].

As described in Sections III-B–D, we suggest that the degradation detected in the extended thermal cycling test is due to a solder bond failure (followed by bypass diode failure), which is most probably caused by an inadequate soldering process. Our previous reports also suggest that the solder bond failure is not induced by the thermomechanical stress if the solder bonding between the busbar and interconnecting ribbon is of good quality, i.e., the solder-bond failures were detected after more than 2500 cycles [31], [32]. In addition, two findings support this suggestion; first, the evolution of dark areas in the EL images and the elevation of temperatures in the IR images within the PV cells in the degraded PV modules were observed on a particular side of two tab-lines in all individual modules of a model as shown in Figs. 9–11. Second, this type of failure was not detected in most models of the tested PV modules, despite the fact that most of them apparently use similar soldering technology. Based on these findings and the reported experience for the factory audit [33], [34], we conclude that the solder bond failure observed in this study was due to the incorrect control of the cell-stringing process, and suggest that the failure caused by this mismanagement would be detected by the extension of the number of cycles (400 or 600 cycles) as it cannot be detected by the standard test of 200 thermal cycles as specified in IEC 61215: 2005. Furthermore, we assume that this type of solder bond failure would be prevented by a well designed and implemented quality management system according to IEC Technical Specification "Guideline for increased confidence in PV module design qualification and type approval (IEC/TS 62941)" with the extended thermal cycling test (600 cycles) as its reliability testing specification [35].

Recently, Bosco et al. reported that the durability of solder bonding, in PV modules with conventional architecture, to thermal fatigue could be estimated by a finite element model simulation of these PV modules under localized ambient weather conditions. They calculated that the solder-fatigue damage accumulated over 25 years in a hot climate zone such as Chennai (India) corresponded to ca., 630 cycles of the thermal cycling

test defined in the IEC 61215 standard [36]. If their simulation is accepted, the PV modules (models E, I, and K) with solder-bond failure observed in the present work would not endure the inelastic strain energy accumulated in Chennai for 25 years. However, when other issues (usage of unreliable materials, application of inadequate configurations, etc.) are built into the design process of PV modules, similar degradation would be also observed over 400 or 600 cycles of thermal cycling tests as it was reported that the thickness of the PV cell and copper in the interconnecting ribbon would significantly affect the accumulation of thermal-fatigue damage in solder during the thermal cycling test, as with thickness of the solder layer between the copper-ribbon and PV cell, which is subjected to the cell-stringing process [37]. Therefore, to clarify whether the solder bond failure observed in the extended thermal cycling test depends on a quality-control issue or not, we should carefully analyze the degradation profiles in multiple samples of a PV module model, as carried out in this study. However, since the duration required in the extended thermal cycling test is so long (400 and 600 cycles correspond to 1600 and 2400 h, respectively, even when the cycle time falls within 4 h), other testing protocols that are modified from the conventional thermal cycling test are required in a short-term judgment [31], [32], [38]–[43]. Consequently, the lifetime prediction test based on Bosco's proposal would be more effective on a sample that has eliminated quality-control issues through these screening tests, for the precise estimation of service lifetime in the field [36], [37].

In the field, PV modules with quality-control issues in solder bonding would not generate their expected electric power before the end of the service lifetime predicted by their own design, i.e., this failure may be corresponding to the "midlife-failure" defined in a review, but not to "wear-out failure" [12]. The solder bond failure induced by the thermal fatigue during the extended thermal cycling test was reported with a distinguishing pattern along with tab-lines in EL/IR images of PV modules [6], [10]–[12], [16], [18], [22], [31]. In our present study, this failure was also detected by these imaging techniques, and we confirmed the increase in the value of $R_s$ in the degraded PV modules by the extraction of their electric parameters from their *I–V* curves under the illuminated conditions, as shown in Figs. 7 and 8. In addition, the increase in the apparent value of $n$ can be simultaneously detected in these degraded PV modules. Owing to the fact that the increase of $R_s$ and the apparent $n$ in a PV cell was elucidated as evidence for the occurrence of nonuniform contact resistance [29], these increases of $R_s$ and apparent $n$ would reflect the variable power-collection caused by solder bond breakdown between the busbar and interconnecting ribbon, which is observed somewhere within the degraded PV modules. It is suggested that this type of failure (as a typical "midlife-failure") would be easily detected in the PV modules installed in the field, by the extraction of PV parameters from their *I–V* curves obtained under illuminated conditions.

## V. CONCLUSION

We carried out an extensive testing of recently manufactured PV modules (13 models) to elucidate their durability to thermomechanical stress, through extended thermal cycling testing. Although 10 out of the 13 models were durable against the thermomechanical stress, induced by the thermal cycling test (600 cycles), three models of PV modules were degraded by the application of this stress. It was revealed that these degradations were caused by solder bond failure between the busbar and interconnecting ribbon on the PV cells, and by bypass-diode shunting, likely to be induced by this solder bond failure. Solder bond failure seems to occur due to inappropriate management and control of the cell-stringing process. Therefore, we concluded that extending the thermal cycling test up to 600 cycles was effective, not only in detecting a quality-control issue caused by an incorrect manufacturing process but also in the estimation of service lifetime in various fields. Consequently, the precise estimation of the design lifetime of these PV modules should be carried out under the conditions that interferences due to quality-control issues were eliminated.

## REFERENCES

[1] IEA PVPS Task1 Team, "Trends 2016 in photovoltaic applications," Int. Energy Agency, Paris, France, 2016.

[2] S. Kurtz *et al.*, "Three-prong path to comprehensive technical standards for photovoltaic reliability," in *Proc. 40th IEEE Photovolt. Spec. Conf.*, 2014, pp. 0919–0924.

[3] S. Kurtz *et al.*, "Moving toward quantifying reliability - The next step in a rapidly maturing PV industry," in *Proc. 42nd IEEE Photovolt. Spec. Conf.*, 2015, pp. 1–8.

[4] D. L. King, M. A. Quintana, J. A. Kratochvil, D. E. Ellibee, and B. R. Hansen, "Photovoltaic module performance and durability following long-term field exposure," *Prog. Photovolt. Res. Appl.*, vol. 8, no. 2, pp. 241–256, Mar. 2000.

[5] M. A. Quintana, D. L. King, T. J. McMahon, and C. R. Osterwald, "Commonly observed degradation in field-aged photovoltaic modules," in *Proc. 29th IEEE Photovolt. Spec. Conf.*, 2002, pp. 1436–1439.

[6] A. Skoczek, T. Sample, and E. D. Dunlop, "The results of performance measurements of field-aged crystalline silicon photovoltaic modules," *Prog. Photovolt. Res. Appl.*, vol. 17, no. 4, pp. 227–240, Jun. 2009.

[7] J.-S. Jeong, N. Park, and C. Han, "Field failure mechanism study of solder interconnection for crystalline silicon photovoltaic module," *Microelectron. Reliab.*, vol. 52, nos. 9–10, pp. 2326–2330, Sep. 2012.

[8] K. Kato, "PVRessQ! PV module failures in the field," in *Proc. Photovolt. Module Reliab. Workshop 2012*, 2012, pp. 13–36. [Online]. Available: http://www.nrel.gov/docs/fy14osti/60169.pdf

[9] E. Hasselbrink *et al.*, "Validation of the PVLife model using 3 million module-years of live site data," in *Proc. 39th Photovolt. Spec. Conf.*, 2013, pp. 7–12.

[10] "Progress reports in the consortium study II on fabrication and characterization of solar cell modules with long life and high reliability (in Japanese)," Nat. Inst. Adv. Ind. Sci. Technol., Tsukuba, Japan, 2012.

[11] A. Pozza and T. Sample, "Crystalline silicon PV module degradation after 20 years of field exposure studied by electrical tests, electroluminescence, and LBIC," *Prog. Photovolt. Res. Appl.*, vol. 24, no. 3, pp. 368–378, Mar. 2016.

[12] IEA-PVPS Task13 Team, "Review of failures of photovoltaic modules," Int. Energy Agency, Paris, France, 2014.

[13] D. C. Jordan and S. R. Kurtz, "Photovoltaic degradation rates -an analytical review," *Prog. Photovolt. Res. Appl.*, vol. 21, no. 1, pp. 12–29, Jan. 2013.

[14] C. R. Osterwald, J. Pruett, S. Rummel, A. Anderberg, and L. Ottoson, "Forward-biased thermal cycling: A new module qualification test," in *Proc. 2000 Nat. Center Photovolt. Program Rev. Meeting*, 2000, pp. 65–66.

[15] J. H. Wohlgemuth, D. W. Cunningham, A. M. Nguyen, and J. Miller, "Long term reliability of PV modules," in *Proc. 20th Eur. Photovolt. Sol. Energy Conf. Exhib.*, 2005, pp. 1942–1946.

[16] J. H. Wohlgemuth, D. W. Cunningham, P. Monus, J. Miller, and A. Nguyen, "Long term reliability of photovoltaic modules," in *Proc. 4th World Conf. Photovolt. Energy Convers.*, vol. 2, 2006, pp. 2050–2053.

[17] J. H. Wohlgemuth *et al.*, "Using accelerated tests and field data to predict module reliability and lifetime," in *Proc. 23rd Eur. Photovolt. Sol. Energy Conf. Exhib.*, 2008, pp. 2663–2669.

[18] W. Herrmann *et al.*, "PV module degradation caused by thermomechanical stress: Real impacts of outdoor weathering versus accelerated testing in the laboratory," in *Proc. SPIE Reliab. Photovolt. Cells, Modules, Compon., Syst. Conf.*, 2010, Paper 77730I.

[19] A. F. Dethlefsen, "Multi-crystalline silicon solar cell modules: crack formation and development due to climate chamber thermal cycle testing," in *Proc. Photovolt. Module Reliab. Workshop 2011*, 2011, p. 1002. [Online]. Available: http://www.nrel.gov/docs/fy14osti/60170.pdf.

[20] A. Funcell, "'The thresher test': Crystalline silicon terrestrial photovoltaic (PV) modules long term reliability and degradation," presented at the *1st Int. PV Module Qual. Assur. Forum*, San Francisco, CA, USA, Jul. 2011.

[21] S. D. Kim *et al.*, "High reliability of SunPower modules with >20% efficiency," in *Proc. 26th Eur. Photovolt. Sol. Energy Conf. Exhib.*, 2011, pp. 3103–3106.

[22] B. Jaeckel *et al.*, "A new standard for holistic quality assurance," in *Proc. 26th Eur. Photovolt. Sol. Energy Conf. Exhib.*, 2011, pp. 3484–3490.

[23] T. Geipel, J. Möller, Y. Zemen, S. Pingel, and J. Berghold, "Results of improved thermal cycle testing of crystalline solar modules," in *Proc. 26th Eur. Photovolt. Sol. Energy Conf. Exhib.*, 2011, pp. 3517–3522.

[24] *Crystalline Silicon Terrestrial Photovoltaic (PV) Modules: Design Qualification and Type Approval,* IEC 61215: 2005, 2005.

[25] *Solar Photovoltaic Energy Systems - Terms, Definitions and Symbols*, IEC TS 61836, 2016.

[26] C. Zhang, J. Zhang, Y. Hao, Z. Lin, and C. Zhu, "A simple and efficient solar cell parameter extraction method from a single current-voltage curve," *J. Appl. Phys.*, vol. 110, no. 6, Sep. 2011, Art. no. 64504.

[27] S. Suzuki *et al.*, "Acceleration of potential-induced degradation by salt-mist preconditioning in crystalline silicon photovoltaic modules," *Jpn. J. Appl. Phys.*, vol. 54, no. 8S1, Aug. 2015, Art. no. 08KG08.

[28] C. A. Schneider, W. S. Rasband, and K. W. Eliceiri, "NIH Image to ImageJ: 25 years of image analysis," *Nature Methods*, vol. 9, no. 7, pp. 671–675, Jul. 2012.

[29] A. S. H. van der Heide, A. Schönecker, J. H. Bultman, and W. C. Sinke, "Explanation of high solar cell diode factors by nonuniform contact resistance," *Prog. Photovolt. Res. Appl.*, vol. 13, no. 1, pp. 3–16, Jan. 2005.

[30] J. Wohlgemuth and S. Kurtz, "International PV QA Task Force's proposed comparative rating system for PV modules," in *Proc. SPIE 9179, Reliab. Photovolt. Cells, Modules, Compon., Syst. VII*, 2014, Paper 917902.

[31] Y. Aoki, M. Okamoto, A. Masuda, T. Doi, and T. Tanahashi, "Early failure detection of interconnection with rapid thermal cycling in photovoltaic modules," *Jpn. J. Appl. Phys.*, vol. 51, no. 10S, Oct. 2012, Art. no. 10NF13.

[32] T. Tanahashi *et al.*, "In situ ac impedance measurement in c-Si PV modules during rapid thermal cycling test," presented at the *2015 NREL Photovolt. Reliab. Workshop*, Golden, CO, USA, Feb. 2015.

[33] P. Rusch and I. Gregory, "Reducing investment risk in PV projects," Solar Business Focus, Feb. 2013.

[34] I. Gregory, "An independent auditor's view on manufacturing QMS," presented at the *2015 NREL Photovolt. Reliab. Workshop*, Golden, CO, USA, Feb. 2015.

[35] *Terrestrial Photovoltaic (PV) Modules - Guideline for Increased Confidence in PV Module Design Qualification and Type Approval*, IEC/TS 62941, 2016.

[36] N. Bosco, T. J. Silverman, and S. Kurtz, "Climate specific thermomechanical fatigue of flat plate photovoltaic module solder joints," *Microelectron. Reliab.*, vol. 62, pp. 124–129, Jul. 2016.

[37] N. Bosco, T. J. Silverman, and S. Kurtz, "The influence of PV module materials and design on solder joint thermal fatigue durability," *IEEE J. Photovolt.*, vol. 6, no. 6, pp. 1407–1412, Nov. 2016.

[38] Y. Meydbray, K. Wilson, E. Brambila, A. Terao, and S. Daroczi, "Solder joint degradation in high efficiency all back contact solar cells," in *Proc. 22nd Eur. Photovolt. Sol. Energy Conf. Exhib.*, 2007, pp. 2561–2564.

[39] G. Cuddalorepatta *et al.*, "Durability of Pb-free solder between copper interconnect and silicon in photovoltaic cells," *Prog. Photovolt. Res. Appl.*, vol. 18, no. 3, pp. 168–182, May 2010.

[40] Y. Zemen, T. Prewitz, T. Geipel, S. Pingel, and J. Berghold, "The impact of yield strength of the interconnector on the internal stress of the solar cell within a module," in *Proc. 25th Eur. Photovolt. Sol. Energy Conf. Exhib./5th World Conf. Photovolt. Energy Convers.*, 2010, pp. 4073–4078.

[41] T. Tanahashi, "Thermal cycling combined with dynamic mechanical load: Preliminary report," in *Proc. Photovolt. Module Reliab. Workshop 2013*, 2013, p. 125. [Online]. Available: http://www.nrel.gov/docs/fy14osti/60167.pdf.

[42] M. Fujimori, T. Kohno, Y. Tsuno, and K. Morita, "Highly accelerated thermal cycling test for short term examination of photovoltaic module reliability," in *Proc. 31st Eur. Photovolt. Sol. Energy Conf. Exhib.*, 2015, pp. 1911–1914.

[43] A. Masuda *et al.*, "Sequential and combined acceleration tests for crystalline Si photovoltaic modules," *Jpn. J. Appl. Phys.*, vol. 55, no. 4S, 2016, Art. no. 04ES10.